Observation of High Angular Momentum Excitons in Cuprous Oxide

J. Thewes, J. Heckötter, T. Kazimierczuk,[†] M. Aßmann, D. Fröhlich, and M. Bayer[*]
Experimentelle Physik 2, Technische Universität Dortmund, D-44221 Dortmund, Germany

M. A. Semina and M. M. Glazov
Ioffe Institute, Russian Academy of Sciences, 194021 St. Petersburg, Russia

(Received 13 March 2015; published 8 July 2015)

The recent observation of dipole-allowed P excitons up to principal quantum numbers of $n = 25$ in cuprous oxide has given insight into exciton states with unprecedented spectral resolution. While so far the exciton description as a hydrogenlike complex has been fully adequate for cubic crystals, we demonstrate here distinct deviations: The breaking of rotational symmetry leads to mixing of high angular momentum F and H excitons with the P excitons so that they can be observed in absorption. The F excitons show a threefold splitting that depends systematically on n, in agreement with theoretical considerations. From detailed comparison of experiment and theory we determine the cubic anisotropy parameter of the Cu_2O valence band.

DOI: 10.1103/PhysRevLett.115.027402 PACS numbers: 78.40.Fy, 71.35.Cc, 78.20.-e, 78.55.-m

Introduction.—Excitonic effects are decisive for the optical properties of semiconductors and insulators [1]. The Coulomb interaction between an electron and a hole leads to a series of bound states, *excitons*, with energies below the band gap. In addition, for the states above the band gap a massive redistribution of oscillator strength towards the low-energy states takes place compared to a free particle description. The description of the bound exciton states by the hydrogenic model has turned out to be extremely successful in this respect, in particular, for bulk semiconductors of cubic symmetry.

For excitons with wave function extensions much larger than the crystal unit cell (the Mott-Wannier excitons) the hydrogen formula for their binding energy, $\mathcal{R}/n^2$ with the Rydberg energy $\mathcal{R}$ in a state of principal quantum number n, can be simply adapted to the solid state case by (i) changing the reduced mass of electron and proton m to that of electron and hole m^*, and (ii) screening the carrier interaction by the dielectric constant ε: $\mathcal{R}^* = \mathcal{R}m^*/(\varepsilon^2\ m)$. The influence of the many-body crystal environment is thus comprised in material properties that for cubic semiconductors are, as a rule, isotropic such as the scalar dielectric constant ε, leading to a formula for excitonic energies that is identical to the one in a system with rotational symmetry.

For the hydrogen problem the spatial symmetry is determined by the continuous rotation group SO(3), where the square of the orbital momentum $L^2 = l(l+1)\hbar^2$ and its z component $L_z = m\hbar$, the magnetic quantum number, are constants of motion, making the problem integrable. Because of this symmetry the energy levels are degenerate with respect to m. For the $1/r$ dependence of the Coulomb potential, the Lenz-Runge vector is also conserved as specific consequence of the underlying SO(4) symmetry, causing the energy level degeneracy in l.

In crystals this rotational symmetry is broken down to discrete groups. For bulk cubic crystals these are the groups O_h or T_d (depending on presence or absence of inversion symmetry). Since both groups represent still quite high symmetry, the deviations from the rotational symmetry are usually captured solely by the lattice-periodic Bloch functions of electron and hole. The envelope wave functions of Mott-Wannier excitons, however, are considered as hydrogenlike involving the spherical harmonics as angular momentum eigenfunctions, even though, strictly speaking, angular momentum is no longer conserved, and l, m are not good quantum numbers. So far, indications for a failure of this description such as observation of a splitting of levels of particular l and mixing of levels with different l have not been reported in the absence of external fields. We note, however, that high angular momentum excitons could be observed in low-dimensional systems by introducing an additional symmetry breaking through external fields. For example, in GaAs-based quantum wells, for which S-like excitons are observed in one-photon absorption, higher angular momentum excitons became accessible by application of magnetic or electric fields [2,3].

Because of the small Rydberg energy in prototype semiconductors like GaAs ($\mathcal{R}^* = 4.2$ meV), consequences of the reduced crystal symmetry are hard to resolve in optical spectra of excitons. One might seek for deviations from the exciton hydrogen model in materials with larger Rydberg energy such as oxides or nitrides, for which possible exciton level splittings, however, may be blurred by crystal inhomogeneities. A somewhat unique position in terms of crystal quality is held by cuprous oxide (Cu_2O) with a Rydberg energy of about 90 meV. The high quality of Cu_2O natural crystals allowed the first experimental demonstration of excitons [4,5], and it is evidenced also

by remarkably narrow absorption lines as highlighted by the observation of the paraexciton in magnetic field with a record linewidth below 100 neV [6].

Here we report a high resolution absorption study of the yellow exciton series in cuprous oxide. Besides the dominant P excitons we resolve exciton triplets from $n = 4$ to 10 with linewidths in the μeV range. These lines are ascribed to F excitons (more precisely, to mixed F and P excitons). Their emergence in the spectra and their splitting which depends systematically on the principle quantum number n are consequences of the reduction from full rotational to discrete O_h symmetry. These findings are in good agreement with calculations in which the band structure details are taken into account.

Symmetry analysis.—The yellow exciton series is associated with transitions between the highest valence and lowest conduction bands in Cu_2O. In this material the topmost valence band corresponds to the irreducible representation $\mathcal{D}_h = \Gamma_7^+$ of the O_h point group, and the bottom conduction band corresponds to $\mathcal{D}_e = \Gamma_6^+$, see Ref. [7] for details. The exciton wave function transforms according to the product $\mathcal{D}_x = \mathcal{D}_e \times \mathcal{D}_h \times \mathcal{D}_r$ where $\mathcal{D}_r$ is the representation describing the wave function of the electron-hole relative motion [8].

In analogy with hydrogen, it is convenient to follow the conventional description and categorize the excitonic states by the symmetry of the relative motion envelope $\mathcal{D}_r$. For S excitons and P excitons $\mathcal{D}_r$ is irreducible, $\mathcal{D}_S = \Gamma_1^+$ and $\mathcal{D}_P = \Gamma_4^-$, respectively, while for the states with higher angular momentum, e.g., the F ($l = 3$) and H ($l = 5$) excitons the representations are reducible, $\mathcal{D}_F = \Gamma_2^- + \Gamma_4^- + \Gamma_5^-$ and $\mathcal{D}_H = \Gamma_3^- + 2\Gamma_4^- + \Gamma_5^-$, showing that l is no longer a good quantum number for cubic symmetry. Still, we will maintain the exciton classification according to orbital angular momentum for simplicity.

To be optically excitable, the exciton state representation $\mathcal{D}_x$ has to contain the three-dimensional $\mathcal{D}_x = \Gamma_4^-$ representation, corresponding to the components of the electric dipole operator. The product of the electron and hole Bloch functions can be decomposed as $\mathcal{D}_e \times \mathcal{D}_h = \Gamma_2^+ + \Gamma_5^+$. Taking into account the envelope function, the resulting P excitons are optically active in one-photon transitions because Γ_4^- is contained in the product representation: $\Gamma_4^- \in \mathcal{D}_P \times \Gamma_5^+$, while this is not the case for the S and D excitons, so that they are dark [9]. The origin of this behavior is the even parity of conduction and valence bands in Cu_2O so that dipole transitions have to involve odd envelopes. However, accounting for the cubic crystal symmetry makes the F and H excitons dipole allowed in addition to the P excitons: One can readily check that the product $\mathcal{D}_F \times \Gamma_5^+$ contains $3\Gamma_4^-$ and $\mathcal{D}_F \times \Gamma_2^+$ contains one more Γ_4^-. Hence F-exciton states can give rise to four spectral lines [10]. Analogously, the product $\mathcal{D}_H \times (\Gamma_2^+ + \Gamma_5^+)$ contains $5\Gamma_4^-$, hence the H exciton can give rise to five lines.

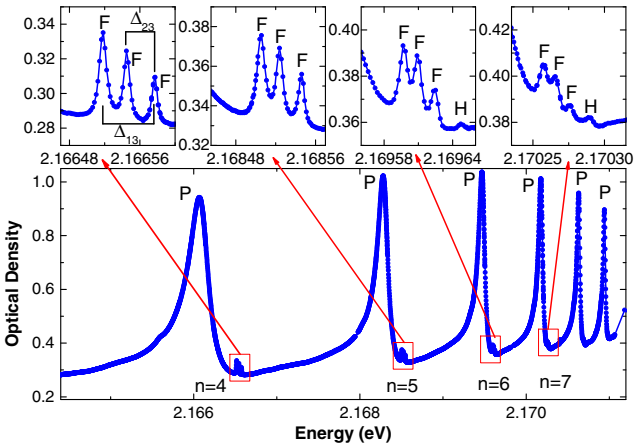

FIG. 1 (color online). Bottom, absorption spectrum of the Cu_2O yellow exciton series in the energy range of states with principal quantum numbers from $n = 4$ to $n = 9$. The top panels show closeups of the high energy flanks of the P excitons with $n = 4, 5, 6$, and 7, respectively.

Experimentals.—To test these predictions, high-resolution absorption spectra were recorded by detecting the intensity of a frequency-stabilized laser with 1 neV linewidth (corresponding to about 250 kHz bandwidth) after transmission through a 30 μm thick Cu_2O crystal slab. The wavelength of the laser emission was scanned in the range of interest from 570 to 580 nm, for details see Ref. [9]. The sample was held in liquid helium at a temperature of 1.2 K and was strain-free mounted in a holder that allowed also application of an electric field along the optical axis.

The bottom panel of Fig. 1 shows an absorption spectrum of the yellow exciton series in the energy range corresponding to principal quantum numbers from $n = 4$ to $n = 9$ (the states with $n = 2$ and 3 are observed below the plotted range). The spectrum is dominated by strong absorption features of the P excitons. The absorption line shape and the exciton binding energy are discussed in detail in Ref. [9]. However, on the high energy flank of these lines weak additional features appear. We highlight that these features can be observed starting from $n = 4$ only. The top panels show closeups of the high energy flanks of the $n = 4, 5, 6$, and 7 P excitons. Each group of features consists of a triplet of lines with the splitting between them decreasing systematically with increasing n. The width of each line is in the μeV range, also decreasing with n which corresponds to lifetimes in the nanosecond range. Starting from $n = 6$ another feature appears on the high energy side of the triplet, approaching the triplet with increasing principal quantum number.

For $n > 7$ the triplet is too close to the P excitons to be resolved in absolute transmission. Thus, we have applied modulation spectroscopy by recording the differential absorption with and without an electric field applied. Only small fields of 15 V/cm or less are applied to avoid notable modifications both of absolute exciton energies as

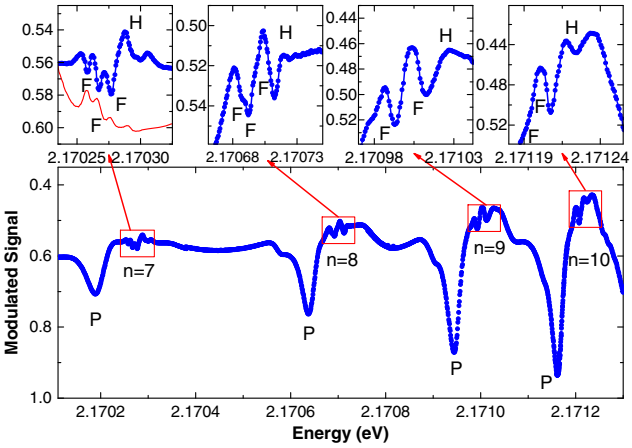

FIG. 2 (color online). Modulation spectra recorded as a difference of transmission with and without a small electric field applied. The electric field strength is 15 V/cm. The bottom panel shows the spectral range of excitons from $n = 7$ up to 10; the top panels give closeups of the corresponding F-exciton features. The red line denotes the transmission spectrum for $n = 7$.

well as splittings between them. The bottom panel in Fig. 2 shows such a modulation spectrum, in which the triplets can be seen up to higher principal quantum numbers. For comparison with Fig. 1, the energy range around the $n = 7$ exciton is shown, where one recognizes the triplet at the same energies as before. For $n = 8$, also the triplet can be seen. However the two low energy lines have almost merged, while the high energy line is still well separated from them. For higher n only a doublet of lines can be seen, as the splitting between the low energy lines is comparable or smaller than their line widths. The peaks in absorption and modulation spectra only appear at the same spectral positions for low fields, temperatures, and exciton densities. Because of the very different size and sensitivity to external fields of Rydberg excitons with different n, we recorded a series of modulation spectra for different fields. With lower fields, the peak positions converge towards a saturation value that agrees with the exciton energy seen in absorption [17].

The angular momentum of exciton states belonging to a particular n is limited by $n - 1$; hence, in the hydrogen model the F states appear only for $n \geq 4$. Since the observed triplet indeed emerges in Fig. 1 starting from $n = 4$ only, we therefore assign it to F excitons. We note that based on the symmetry considerations presented above, F excitons belonging to a particular n are expected to appear in optical spectra as a quadruplet. The numerical calculations presented below confirm this and demonstrate that one of the lines is indeed substantially weaker as compared with three others. Moreover, its energy is close to that of one strong line. For additional confirmation, experiments in moderate magnetic fields [12] were carried out that demonstrate a splitting into eight lines, of which six show non-negligible oscillator strength in small fields below 1.25 T, in agreement with our symmetry analysis which predicts a twofold splitting of each line in the triplet. Furthermore, the additional feature emerging from $n = 6$ onwards can be attributed to H excitons. Their expected splitting is, however, too small to be resolved.

To the best of our knowledge, such high angular momentum exciton states including their fine structure splitting have not been resolved so far without applying external fields. We emphasize here that the description as a hydrogenlike complex can explain neither the optical absorption of F and H excitons, nor their splitting. It is therefore a unique signature of the breaking of the rotational symmetry in the cubic crystal and a consequence of its discrete symmetry.

Microscopic theory.—In Cu_2O the excitonic Rydberg $\mathcal{R}^* \approx 90$ meV and the splitting between the Γ_7^+ and Γ_8^+ valence bands $\Delta \approx 130$ meV have the same order of magnitude. Therefore, a consistent theory of excitonic states has to be based on treating the complex valence band structure and the Coulomb interaction on the same level. Following Ref. [7] we present the exciton Hamiltonian (for zero center-of-mass wave vector) as

$$\mathcal{H} = \frac{p^2}{\hbar^2} - \frac{2}{r} - \frac{\mu}{3\hbar^2}(P^{(2)} \cdot I^{(2)}) + \frac{2}{3}\bar{\Delta}(1 + \boldsymbol{I} \cdot \boldsymbol{s}_h) + \mathcal{H}_c. \quad (1)$$

Here $\boldsymbol{p}$ is the momentum of the relative electron-hole motion, $\boldsymbol{I}$ is the angular momentum operator for effective spin one acting in the basis of the orbital hole Bloch functions Γ_5^+, and $\boldsymbol{s}_h$ is the hole spin operator ($s_h = 1/2$). The energies are measured in units of the "bulk" excitonic Rydberg $\mathcal{R}^* = e^4 m_0/(2\hbar^2\varepsilon^2\gamma_1')$, the distances are measured in units of the corresponding Bohr radius, $a^* = \hbar^2\varepsilon\gamma_1'/(e^2 m_0)$, ε is the static dielectric constant, $\bar{\Delta} = \Delta/\mathcal{R}^*$ is the dimensionless splitting between the Γ_7^+ and Γ_8^+ bands, $\gamma_1' = \gamma_1 + m_0/m_e$, $\mu = (6\gamma_3 + 4\gamma_2)/(5\gamma_1')$, m_e is the conduction electron mass, m_0 is free electron mass, and the γ_i $(i = 1, 2, 3)$ are the Luttinger parameters. In contrast to Ref. [7] we include into Eq. (1) the cubic symmetry terms [18]

$$\mathcal{H}_c = \frac{\delta}{3\hbar^2}\left(\sum_{k=\pm 4}[P^{(2)} \times I^{(2)}]_k^{(4)} + \frac{\sqrt{70}}{5}[P^{(2)} \times I^{(2)}]_0^{(4)}\right), \quad (2)$$

with $\delta = (\gamma_3 - \gamma_2)/\gamma_1'$. This extension is crucial, as our calculations show, to describing the fine structure of F-exciton states absent otherwise. In Eqs. (1) and (2) we use $P^{(2)}$ and $I^{(2)}$ for the second-rank irreducible components of the tensors $p_i p_j$ and $I_i I_j$, where $i, j = x, y, z$ and p_i, I_i are the Cartesian components of $\boldsymbol{p}$ and $\boldsymbol{I}$, respectively. Note that the quartic terms, i.e., $p_x^4 + p_y^4 + p_z^4$, being allowed in O_h, result in a F-P mixing and make the F states active but do not cause their splitting.

The Hamiltonian (1) without cubic contribution $\mathcal{H}_c$ ($\delta = 0$) has full rotational symmetry and already provides a quite accurate description of the P-exciton state energies [7]. Therefore, it is instructive to disregard $\mathcal{H}_c$ and determine the spectrum and wave functions of P and F excitons. Also, the suppressed short-range electron-hole exchange interaction makes it possible to disregard the electron spin and characterize the excitons by the hole total momentum F and its z component F_z, where $\boldsymbol{F} = \boldsymbol{J} + \boldsymbol{L}$ is the sum of the momentum of the hole Bloch functions $\boldsymbol{J} = \boldsymbol{s}_h + \boldsymbol{I}$ and the envelope function orbital momentum $\boldsymbol{L}$.

The P envelopes of excitons correspond to $F = 1/2$ and $F = 3/2$ states [7], while F excitons correspond in this approximation to $F = 5/2$ and $7/2$, respectively. With inclusion of the cubic symmetry, F and F_z are no longer good quantum numbers. In particular, the $F = 5/2$ state gives rise to Γ_6^- and Γ_8^- states while $F = 7/2$ gives rise to Γ_6^-, Γ_7^-, and Γ_8^- states. Note that Γ_6^- and Γ_8^- are optically active ($\Gamma_4^- \in \Gamma_6^- \times \mathcal{D}_e$, $\Gamma_8^- \times \mathcal{D}_e$), while the Γ_7^- states are dark. States of the same symmetry have to be treated as close to degenerate, see Refs. [12] and [18] for details. Following the methods of Refs. [7,19,20], see Supplemental Material [12] for details, we have calculated the energy spectrum of the P and F excitons for different values of the cubic anisotropy parameter δ keeping all other parameters known from literature fixed. Our calculations show that the reasonably small value of $\delta = -0.1$ gives good accord with the experiment [12]. In this case, two optically active states out of four have very close energies. Moreover, one of those states, namely, Γ_6^- originating from $F = 7/2$, has small oscillator strength [12]. Smaller (larger) values of δ result in too small (large) predictions for the F-shell splitting, so that the estimate of δ from the experimental data is quite accurate.

Discussion.—Figures 3(a) and 3(b) compare the results of calculations of the P-exciton binding energy and the splitting between F and P excitons as a function of principal quantum number n (the solid lines connect calculated values for discrete n) with the measured data (dots), and serve as reference for the accuracy of the description of the exciton states by our model. For the F excitons we have calculated the center of gravity of the F-exciton lines. The comparison shows excellent agreement between theory and experiment, providing confidence that also the μeV splittings between the F excitons can be assessed by our model.

These splittings are shown in Fig. 3(c), where Δ_{13} is the energy separation between the outermost levels and Δ_{23} is the energy separation between the middle and higher energy level, see Fig. 1. Note, that the calculated energy of the fourth state with weak oscillator strength coincides within the accuracy of several percent with the energy of the middle state in the triplet. The points with $4 \le n \le 7$ were measured in absolute transmission (see Fig. 1), while the points with $n \ge 8$ were taken from modulation spectroscopy. Both magnitudes of the splittings and their

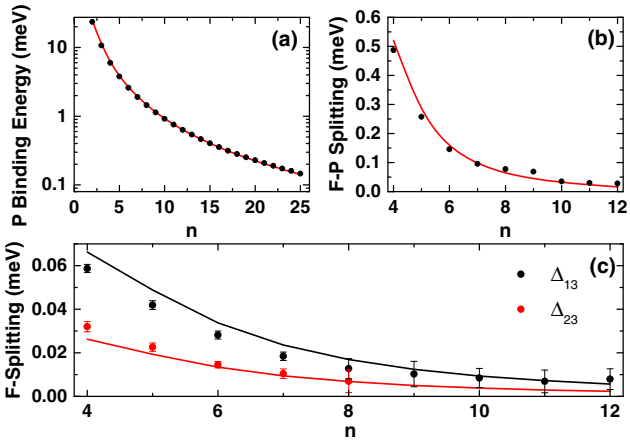

FIG. 3 (color online). Comparison of theoretical calculations and experimental data for P-exciton binding energy (a), splitting between F and P excitons (b), and splittings of F triplet as defined in Fig. 1(c) vs principal quantum number. Dots give experimental data. Theory is shown by lines connecting calculated data for discrete values of n. The parameters of the calculation are $\mathcal{R}^* = 87$ meV, $\mu = 0.47$, $\Delta = 134$ meV [7], and $\delta = -0.1$.

dependence on n are in good agreement with our calculations. The splitting between the states decreases strongly with n, as higher-n states are more extended in space so that their wave function averages over more crystal unit cells and becomes less sensitive to crystal symmetry deviations from the full rotation group. More quantitatively, the decrease is due to the fact that the states are intermixed by quadratic combinations of the momentum operator $p_i p_j$. The corresponding interaction matrix elements scale as the inverse square of the state radii. In the hydrogen model $\langle r^{-2} \rangle \propto n^{-3}(l+1)^{-1}$, indicating that the splittings for higher angular momentum states decrease with n and l. This explains the unresolved splitting of the H excitons in absorption.

The agreement of the developed model with the experimental data allows us to accurately evaluate the valence band parameters in Cu_2O. Taking the static dielectric constant $\varepsilon = 7.5$ [21], the electron effective mass $m_e = 0.99 m_0$ [22], and using our values for $\mathcal{R}^*$, μ, and δ, we obtain the following values of the Luttinger parameters: $\gamma_1 = 1.79$, $\gamma_2 = 0.82$, and $\gamma_3 = 0.54$. Interestingly, in this material $\gamma_3 < \gamma_2$, which is also indicated by microscopic calculations [12,23]. We emphasize that the obtained Luttinger parameters may serve as a benchmark for theoretical models of the Cu_2O band structure.

Conclusion.—In summary, we have discovered high angular momentum exciton states in one-photon absorption spectra of high-quality Cu_2O bulk crystals. Observation of these states becomes possible through the rotational symmetry breakdown by the cubic crystal environment. Even though this symmetry breaking is weak due to the high O_h symmetry, the resulting level splittings could be resolved

because of the for crystals record-low absorption feature linewidths. Our results open the path towards investigating further aspects of Rydberg excitons. Inspired from Rydberg atoms, it may become possible to investigate the semiconductor equivalent of the highly sensitive circular states. Further, the large number of observed levels may enable us to perform a statistical treatment of energy levels which is the key to investigating the transition of the system towards quantum chaos [24,25].

We acknowledge the support by the Deutsche Forschungsgemeinschaft and the Russian Foundation for Basic Research in the frame of ICRC TRR 160, the RF President Grants No. MD-5726.2015.2, No. NSh-5062.2014.2, and No. NSh-1085.2014.2, RF government Grant No. 14.Z50.31.0021, the Dynasty Foundation, and programs of RAS.

*Also at Ioffe Institute, Russian Academy of Sciences, 194021 St. Petersburg, Russia.

†Institute of Experimental Physics, Faculty of Physics, University of Warsaw, ul. Pasteura 5, 02-093 Warsaw, Poland

[1] See, for example, C. F. Klingshirn, *Semiconductor Optics* (Springer, Berlin, 2012).

[2] L. Viña, G. E. W. Bauer, M. Potemski, J. C. Maan, E. E. Mendez, and W. I. Wang, High angular-momentum excitons in GaAs/$Ga_{1-x}Al_x$As quantum wells, Phys. Rev. B **38**, 10154 (1988).

[3] L. Viña, G. E. W. Bauer, M. Potemski, J. C. Maan, E. E. Mendez, and W. I. Wang, Term spectrum of magneto-excitons in quasi-two-dimensional systems, Phys. Rev. B **41**, 10767 (1990).

[4] E. F. Gross and N. A. Karryjew, Light absorption by cuprous oxide crystal in infrared and visible part of the spectrum, Dokl. Akad. Nauk SSSR **84**, 471 (1952).

[5] E. F. Gross, Optical spectrum of excitons in the crystal lattice, Il Nuovo Cimento **4**, 672 (1956).

[6] J. Brandt, D. Fröhlich, C. Sandfort, M. Bayer, H. Stolz, and N. Naka, Ultranarrow Optical Absorption and Two-Phonon Excitation Spectroscopy of Cu_2O Paraexcitons in a High Magnetic Field, Phys. Rev. Lett. **99**, 217403 (2007).

[7] C. Uihlein, D. Fröhlich, and R. Kenklies, Investigation of exciton fine structure in Cu_2O, Phys. Rev. B **23**, 2731 (1981).

[8] E. L. Ivchenko, *Optical Spectroscopy of Semiconductor Nanostructures* (Alpha Science, Harrow, 2005).

[9] T. Kazimierczuk, D. Fröhlich, S. Scheel, H. Stolz, and M. Bayer, Giant Rydberg excitons in the copper oxide Cu_2O, Nature (London) **514**, 343 (2014).

[10] The transitions to the Γ_2^+ state (paraexciton) are spin forbidden and can be activated by magnetic field [6,11]. Owing to the cubic symmetry, the $\mathcal{D}_F \times \Gamma_2^+$ state mixes with $\mathcal{D}_F \times \Gamma_5^+$ and becomes allowed but remains weak, see Supplemental Material [12] for details.

[11] S. V. Gastev, E. L. Ivchenko, G. E. Pikus, N. S. Sokolov, and N. L. Yakovlev, Polarization of paraexciton luminescence in Cu_2O crystals in magnetic field, Fiz. Tverd. Tela (Leningrad, USSR) **25**, 3002 (1983).

[12] See Supplemental Material at http://link.aps.org/supplemental/10.1103/PhysRevLett.115.027402, which includes Refs. [13–16], for data on magnetic field effect and details on theory.

[13] G. F. Koster, R. G. Wheeler, J. O. Dimmock, and H. Statz, *Properties of the Thirty-Two Point Groups* (MIT Press, Cambridge, MA, 1963).

[14] A. Abragam and B. Bleaney, *Electron Paramagnetic Resonance of Transition Ions*, International Series of Monographs on Physics (Clarendon Press, Oxford, 1970).

[15] D. A. Varshalovich, A. N. Moskalev, and V. K. Khersonskii, *Quantum Theory of Angular Momentum* (World Scientific Publishing, Singapore, 1988).

[16] N. Lipari and A. Baldereschi, Interpretation of acceptor spectra in semiconductors, Solid State Commun. **25**, 665 (1978).

[17] B. V. Shanabrook, O. J. Glembocki, and W. T. Beard, Photoreflectance modulation mechanisms in GaAs-Al_xGa_{1-x}As multiple quantum wells, Phys. Rev. B **35**, 2540 (1987).

[18] A. Baldereschi and N. O. Lipari, Cubic contributions to the spherical model of shallow acceptor states, Phys. Rev. B **9**, 1525 (1974).

[19] A. Baldereschi and N. Lipari, Spherical model of shallow acceptor states in semiconductors, Phys. Rev. B **8**, 2697 (1973).

[20] M. A. Semina and R. A. Suris, Effect of localization in quantum wells and quantum wires on heavy-light hole mixing and acceptor binding energy, Semiconductors **45**, 917 (2011).

[21] O. Madelung, U. Rössler, and M. Schulz, SpringerMaterials: The Landolt-Börnstein Database (http://www.springermaterials.com).

[22] A. Goltzene, C. Schwab, and H. C. Wolf, Carrier resonance in Cu_2O, Solid State Commun. **18**, 1565 (1976); J. W. Hodby, T. E. Jenkins, C. Schwab, H. Tamura, and D. Trivich, Cyclotron resonance of electrons and of holes in cuprous oxide, Cu_2O, J. Phys. C **9**, 1429 (1976).

[23] E. Ruiz, S. Alvarez, P. Alemany, and R. A. Evarestov, Electronic structure and properties of Cu_2O, Phys. Rev. B **56**, 7189 (1997); M. French, R. Schwartz, H. Stolz, and R. Redmer, Electronic band structure of Cu_2O by spin density functional theory, J. Phys. Condens. Matter **21**, 015502 (2009).

[24] See, for example, T. F. Gallagher, Rydberg Atoms, *Cambridge Monographs on Atomic, Molecular and Chemical Physics* (Cambridge University Press, Cambridge, 2005).

[25] L. Viña, M. Potemski, and W. I. Wang, Signatures of quantum chaos in the magneto-excitonic spectrum of quantum wells, Phys. Usp. **41**, 153 (1998).